ELSEVIER

Polymer 41 (2000) 351–356

polymer

Morphologies and mechanical properties of syndiotactic polypropylene (sPP)/ polyethylene (PE) blends

J. Loos[a], M. Bonnet[b], J. Petermann[b,*]

[a]*Eindhoven Polymer Labs., Dutch Polymer Institute, Eindhoven University of Technology, P.O. Box 513, 5600 MB Eindhoven, The Netherlands*
[b]*Department of Chemical Engineering, Institute of Material Science, University of Dortmund, 44221 Dortmund, Germany*

Received 16 July 1998; received in revised form 23 November 1998; accepted 14 January 1999

Abstract

The tensile properties of blends based on syndiotactic polypropylene (sPP) and high-density polyethylene (HDPE) have been studied. In order to understand the unexpected decrease in ductility, the crystallization behavior of these blends was characterized by transmission electron microscopy and in-situ Raman spectroscopy. For all investigated blends demixing occurs, and results for low HDPE concentrations in an island-like morphology of HDPE domains embedded in a continuous sPP matrix. For all investigated sPP/HDPE blends the start temperature of the sPP crystallization significantly increases with increasing HDPE content.

Keywords: Syndiotactic polypropylene/polyethylene blends; Mechanical behavior; Morphology

1. Introduction

The polymerization of isotactic polypropylene (iPP) and syndiotactic polypropylene (sPP) has generally been known since the work of Natta et al. [1], but the properties of sPP have been less well investigated than those of the isotactic configuration. Although, despite interesting properties of sPP as high mechanical ductility and high optical transparency, sPP has enjoyed no such commercial success as iPP.

Besides many other factors, the slow crystallization rate is a main disadvantage for the processing behavior of the material. However, we have reported some drastic changes in the properties of sPP when blended with high-density polyethylene (HDPE) [2]. Especially, the crystallization rate increases approximately by a factor of four using a HDPE concentration of only 1 wt.-%, and more than ten times when blending sPP with 10 wt.-% HDPE.

It is the purpose of this work to report some additional mechanical properties of the blends of sPP and HDPE together with new insights in its morphological characterization.

2. Experimental

The HDPE used in the experiments was Lupolene 6021D from BASF AG Ludwigshafen, Germany, and the sPP was kindly supplied by the Fina Oil and Chemical Company. The mixtures were prepared by solution blending in xylene as a common solvent and acetone as a precipitant. The precipitated powder was dried in vacuum for 12 h and remelted at 150°C. Blend compositions are indicated as sPP [wt.-%]/HDPE [wt.-%].

For tensile drawing, strips of 150 mm in length and 15×2 mm^2 in width and thickness were used with a gauge length of 100 mm and a drawing rate of 2 mm/min (2% min^{-1}). The Young's modulus was determined from the slope of the stress–strain curve between 0.05 and 0.25% strain. The used device was a Zwick universal tensile testing machine Type 7025/5. Mechanical data presented in this article are the average of 5 independent measurements.

Thin cross-sectional cryo-microtom cuts of these samples were used for transmission electron microscope (TEM) investigations after a ruthenium oxide (RuO_4) staining preparation [3,4]. TEM was performed using a Philips CM200 operated at 200 kV and a Jeol 2000FX operated at only 80 kV in order to enhance the contrast.

The device used for in-situ Raman spectroscopy was a Dilor Labram system equipped with a Linkam THMS 600 hotstage. Measurements were carried out with a cooling

* Corresponding author. Present address: Institute of Material Science, Department of Chemical Engineering, University of Dortmund, 44221 Dortmund, Germany. Tel.: + 49-231-755-2479; fax: + 49-231-755-2480.

0032-3861/00/$ - see front matter
PII: S0032-3861(99)00092-0

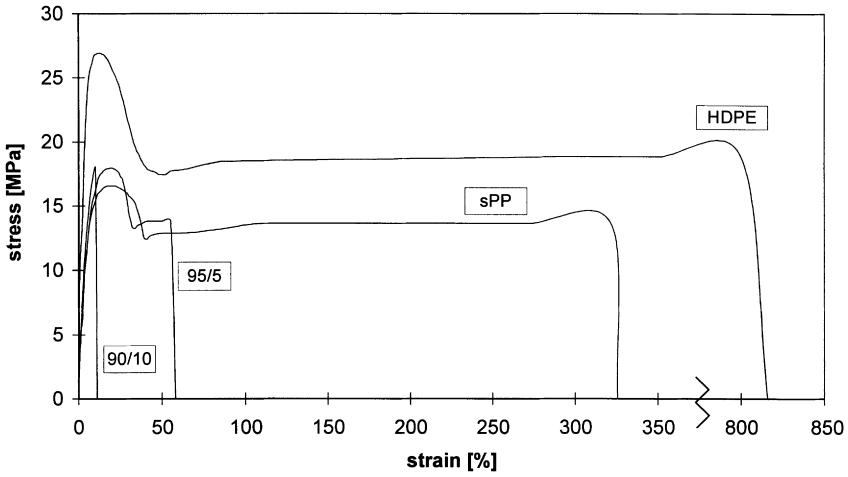

Fig. 1. Stress–strain curves for sPP, HDPE and blends containing 5 and 10 wt.-% HDPE.

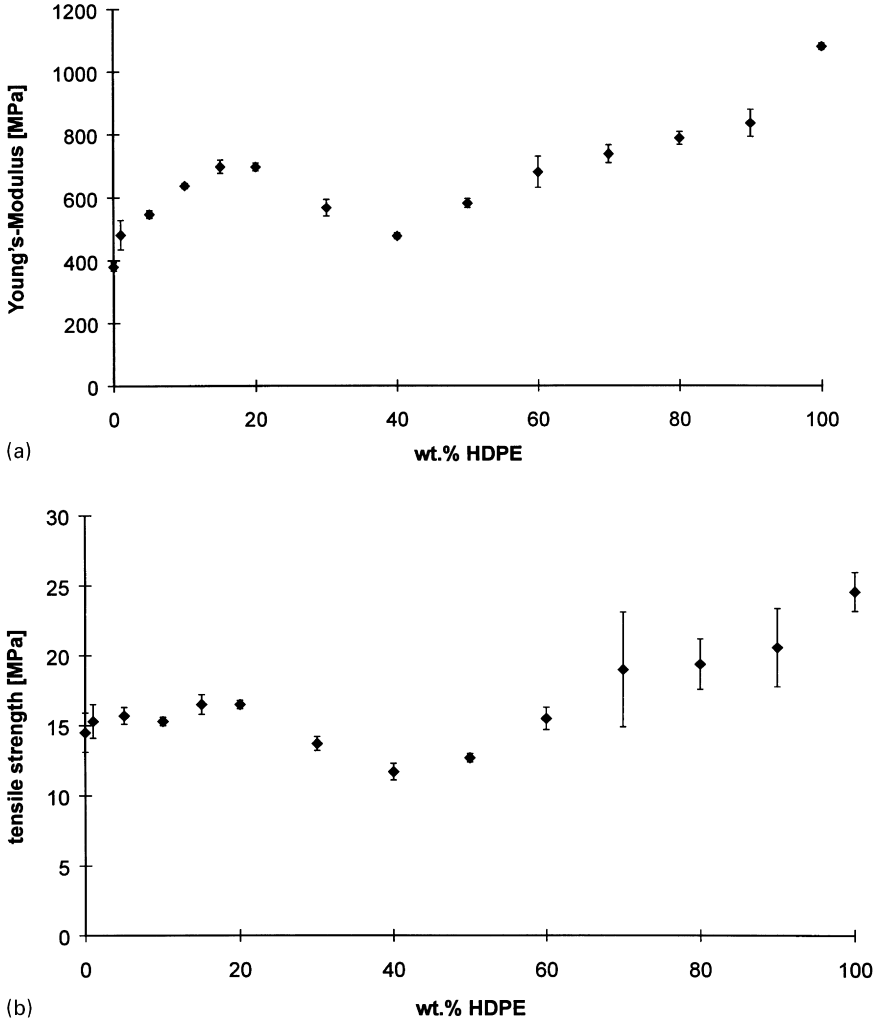

Fig. 2. (a) Young's modulus and (b) tensile strength for sPP, HDPE and blends with different HDPE concentrations.

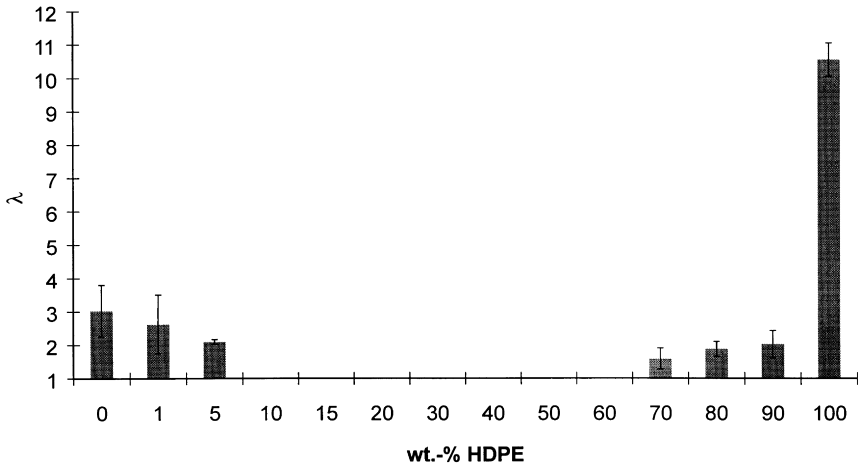

Fig. 3. Maximum achievable λ for sPP, HDPE and blends with different HDPE concentrations.

rate of 2°C/min from the melt at 150°C to RT, and single data scans were collected every 30 s followed by delay time of 30 s. Internal calibration of the Raman spectrometer was performed using the silicon band at 520.7 cm^{-1}.

3. Results and discussion

3.1. Tensile testing

In Fig. 1, the stress–strain curves of sPP, HDPE and

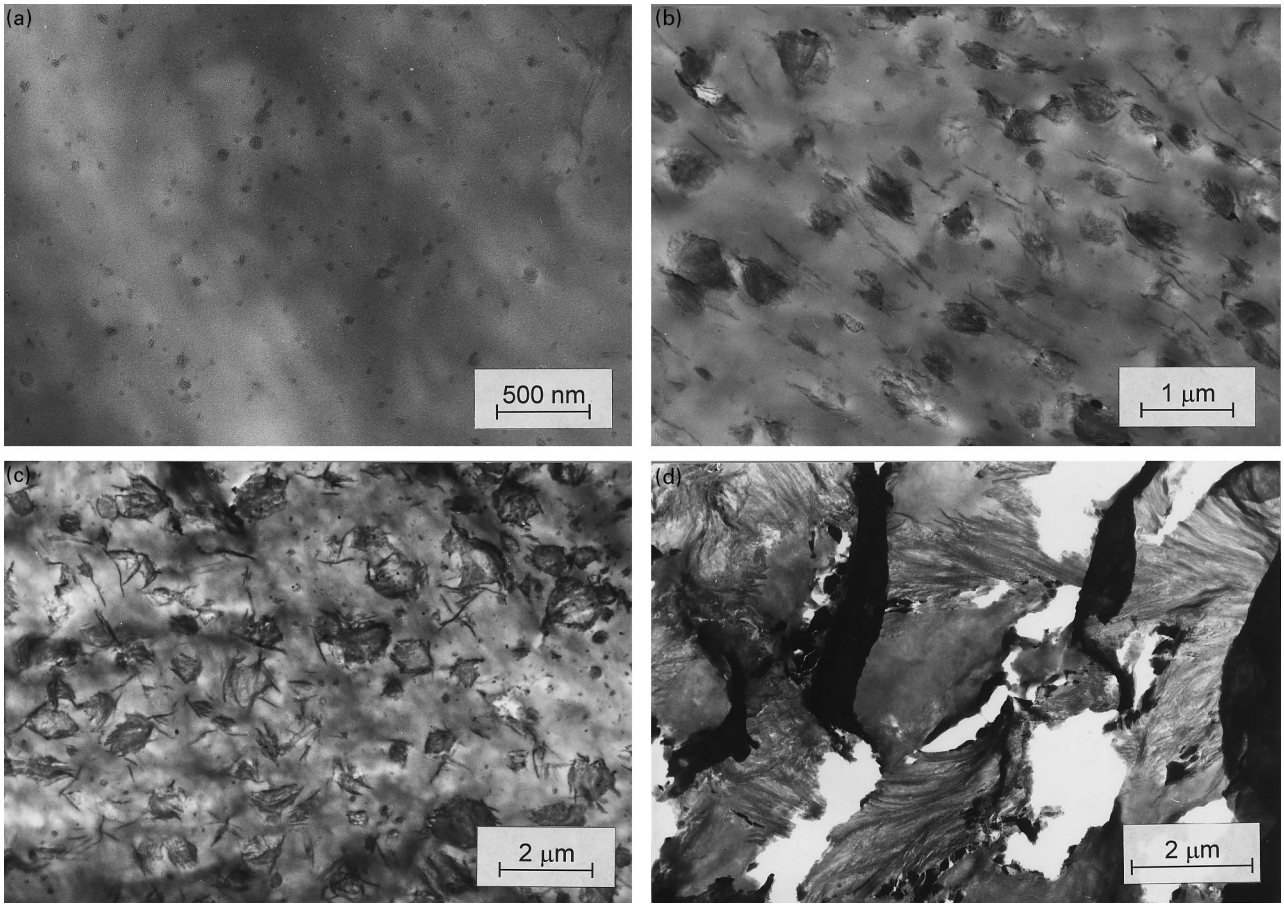

Fig. 4. Transmission electron brightfield micrographs of sPP/HDPE blends with several concentrations of HDPE: (a) 1 wt.-% (b) 10 wt.-% (c) 20 wt.-% (d) 50 wt.-%.

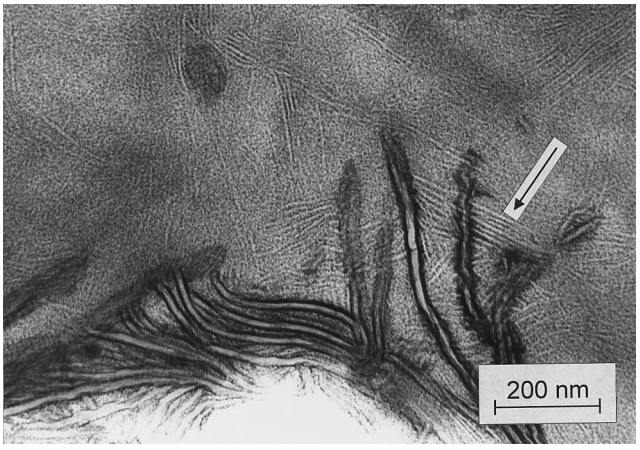

Fig. 5. Transmission electron brightfiled micrograph of a sPP/HDPE interface (20 wt.-% HDPE). The arrow marks several single sPP lamellae growing on the surface of a PE lamellar crystal.

blends containing 5 and 10 wt.-% HDPE are plotted. Both, pure sPP and pure HDPE show usual plastic deformation via necking with elongations $\epsilon \approx 300-800\%$. But already for samples containing only 5 wt.-% HDPE, the drawing behavior of the blends changes, and for the 90/10 blend samples, brittle fracture takes place before necking after approximately 10% elongation. Fig. 2 shows the Young's modulus (Fig. 2(a)) and the tensile strength (Fig. 2(b)) as a function of the HDPE-concentration, respectively. For low concentrations of HDPE a synergetic increase in the Young's modulus with a maximum at about 20 wt.-% HDPE is measured, and for blends containing more than 20 wt.-% HDPE a slight decrease in tensile strength is observed. The maximum achievable draw ratio decreases drastically with increasing HDPE concentration, and for HDPE concentrations between 10 and 70 wt.-% no neck formation can be observed (Fig. 3).

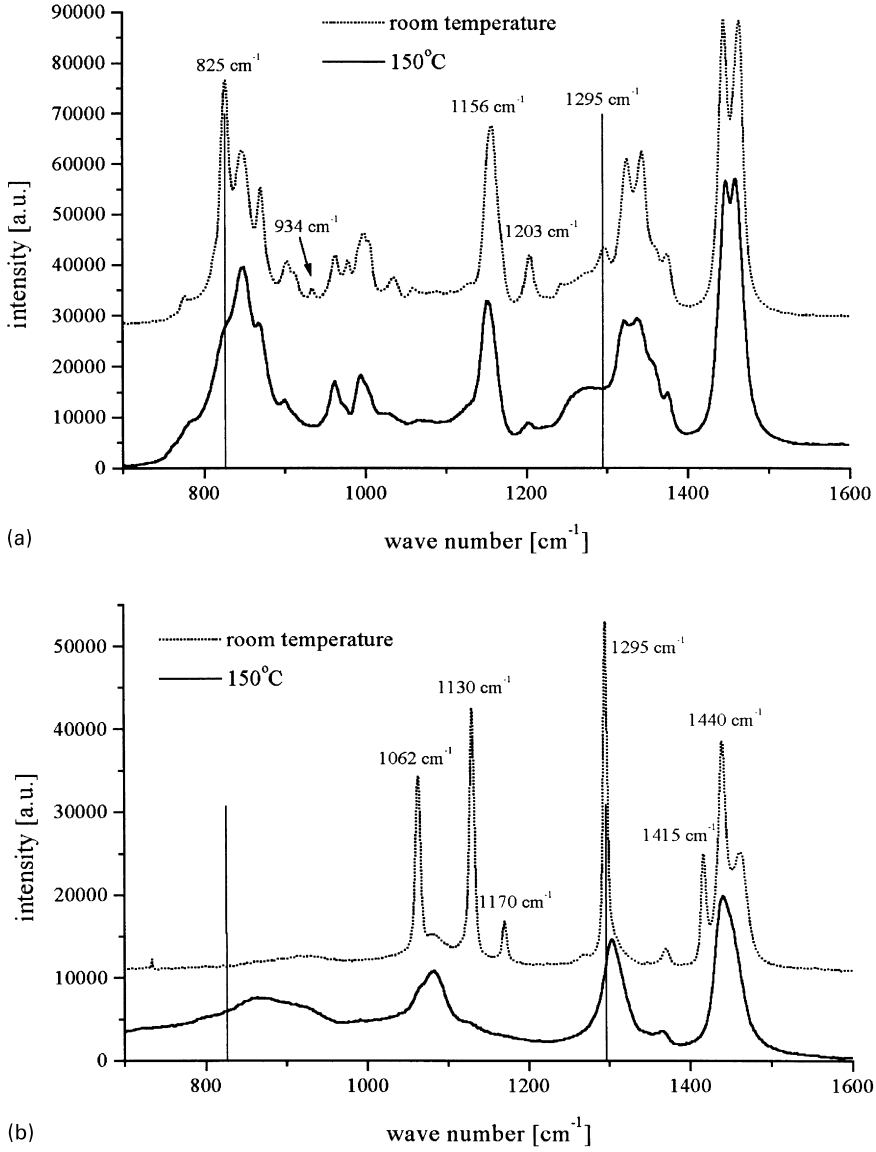

Fig. 6. Raman spectra of (a) sPP and (b) HDPE, in the melt and at room temperature.

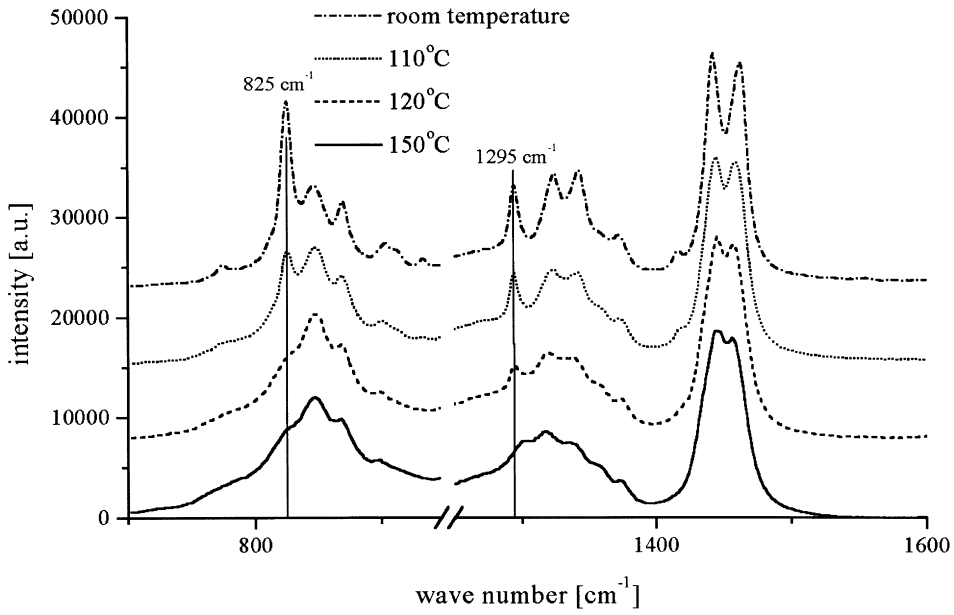

Fig. 7. Raman spectra of a sPP/HDPE blend containing 10 wt.-% HDPE, acquired during crystallization from the melt. Straight lines indicate the wave numbers of 825 cm^{-1} (mixed amorphous and crystalline mode of sPP) and 1295 cm^{-1} (PE crystalline CH_2 twisting).

3.2. Transmission electron microscopy (TEM)

Fig. 4 shows a set of TEM bright-field micrographs of sPP/HDPE blends with several concentrations of HDPE. Using stained samples with in focus conditions of the TEM and a low magnification (Fig. 4(a)–(d)), the dark areas with a lamellar sub-morphology and the brighter areas without visible morphological details can be attributed to HDPE rich and sPP rich areas, respectively. The difference in the contrasts of the two components results from a stronger interaction of the RuO_4 with the HDPE. On higher magnification (Fig. 5), crystalline and amorphous areas can be distinguished from the amorphous areas appearing darker than the crystalline areas due to a higher amount of RuO_4 in the amorphous phases.

Low concentrations of 1, 10 and 20 wt.-% HDPE exhibit demixed island-like HDPE domains in a sPP matrix (Fig. 4(a)–(c)). The size of the domains increases with increasing HDPE concentration. Beside these domains, only a few isolated polyethylene lamellae can be found in the sPP matrix, and hence, there is evidence for a homogeneous distribution of small HDPE domains in the sPP matrix.

The 50 wt.-% HDPE samples show a homogeneous distribution of the domain dimensions, but now the domains of both components, the sPP and the HDPE, are approximately of the same size (Fig. 4(d)). During the sectioning local deformations of these samples have resulted only in the failure of a few interfaces between the sPP and the HDPE domains, but also in failure of the pure components. This observation can be considered as an evidence for good interface adhesion between sPP and HDPE. The black areas in Fig. 4(d) are artifacts caused by the sample preparation.

In a previous study we have reported the drastic increase of the crystallization rate of sPP when blended with polyethylene (PE) [2]. It is known that sPP crystallizes epitaxially onto uniaxially oriented PE films with a very sharp texture [5]. Moreover, from the epitaxy of PE on iPP it is known, that secondary nucleation of the PE on (*hk*0) iPP crystal surfaces causes epitaxy [6–10]. Similar observations were made in the system LDPE/HDPE [11–13]. In the systems mentioned earlier, the epitaxial nucleation accelerates the crystallization process.

Fig. 5 shows a bright-field TEM micrograph of a sPP/HDPE interface (80/20 sample). At the higher magnification more details in the lamellar morphology can be observed. Especially, besides the HDPE crystals with their strongly stained amorphous areas, very thin sPP crystals are visible. Some sPP lamellar crystal bundles and several single sPP lamellae are parallel growing away from the PE crystal surfaces. The parallel alignment of the bundled crystals indicates an oriented nucleation of the sPP on the HDPE crystals. Accordingly, it is speculated that in the sPP/HDPE blends similar mechanisms are acting for the nucleation of the sPP on the HDPE lamellae as in the other epitaxial systems. This implies that the synergisms in mechanical properties are caused by the same mechanisms, the bridging of the sPP amorphous zones by HDPE lamellae [14]. The bridging of the mechanically soft amorphous areas by stiff entities (crystallites) stiffens semicrystalline polymers considerably and also increases their mechanical strength.

3.3. Raman spectroscopy

Fig. 6 presents Raman spectra of the melts and the semicrystalline states of sPP and HDPE, respectively. So far, the vibration modes of sPP were not yet accurately assigned to

Raman band positions in the literature. Following the solidification from the melt of pure sPP, a strong intensity reflecting the increased crystallinity was found at a wave number of 825 cm^{-1} and is marked by a straight line in Fig. 6(a). Additional minor intensities, e.g. at 1203 and 1295 cm^{-1}, reflect the increased crystallinity of the sPP sample after solidification, but in the investigated wave number range only the weak band position at 934 cm^{-1} can be assigned to a pure crystalline vibration mode of sPP. In contrast to sPP the Raman spectrum of PE has been discussed since decades. In the investigated wave number range 700 to 1600 cm^{-1}, all band positions are assigned to certain vibration modes [15–17]. Especially the band position at 1295 and 1304 cm^{-1} correspond to the crystalline and amorphous CH_2 twisting modes of PE, respectively, and the former is marked with a straight line in Fig. 6(b).

Fig. 7 illustrates examples of Raman spectra of a 90/10 blend obtained during the crystallization from the melt. The four spectra represent superpositions of sPP and HDPE spectra as shown in Fig. 6, but all Raman band intensities are weighted corresponding to the blend composition. In the molten state the spectrum shows all characteristic band positions of amorphous sPP. Additionally, the amorphous CH_2 twisting band of PE is visible at approximately 1304 cm^{-1}, and the shape of the sPP bands has changed in the wave number range 1400 to 1500 cm^{-1} caused by overlapping with the CH_2 deformation and bending bands of PE. In the course of HDPE crystallization during the experiment, intensities and band positions alter, which is shown in the Raman spectrum obtained at 120°C. The intensity of the amorphous twisting band of PE decreases, combined with simultaneous growth of the crystalline CH_2 twisting band at 1295 cm^{-1}. The crystallization start temperature of the HDPE content of the blend can be committed to 127°C following the formation of the crystalline CH_2 twisting band.

The spectrum obtained at 110°C shows additional crystallization of the sPP content. Both, the increased intensity at 825 and 934 cm^{-1}, and the separation of the bands in the wave number range 800 to 900 cm^{-1} indicate the crystallization. The growth of intensity at 1295 cm^{-1} corresponds to the complete crystallization of the HDPE content and to the additional appearance of an sPP band located at the same position, as seen in Fig. 6(a). Using a cooling rate of 2°C/min, the initial crystallization temperature of sPP can be committed to 116°C. Finally, at room temperature the further increase of band intensities at 825 and 1295 cm^{-1} shows the complete crystallization of the sample. Using the same condition with 2°C/min cooling rate from the melt, the crystallization start temperature of pure sPP is approximately 104°C as reflected by the growth of the same bands at 825, 934 and 1295 cm^{-1}.

4. Conclusion

The mechanical behavior, morphology and crystallization from the melt of high density polyethylene/syndiotactic polypropylene blends were investigated. The mechanical behavior of the blends changes drastically compared to pure HDPE and sPP, and for HDPE concentrations between 10 and 70 wt.-%, no neck formation is observed. For all investigated blends demixing occurs and results for low HDPE concentrations in a island-like morphology of HDPE domains in a sPP matrix. A good interface adhesion between the phases was observed. Using in-situ Raman spectroscopy, the crystallization of the sPP phase in the blends was investigated. The start temperature of crystallization increases more than 10°C if HDPE is present, which reflects the favored nucleation of sPP in the blends.

Acknowledgements

The financial support of the Deutsche Forschungsgemeinschaft (DFG) is gratefully acknowledged.

References

[1] Natta G, Pasquon I, Corradini P, Peraldo M, Pegoraro M, Zambelli A. Rend Accad Naz Lincei 1960;28:539.
[2] Bonnet M, Loos J, Petermann J. Colloid Polym Sci 1998;276:524.
[3] Trent JS, Scheinbeim JI, Couchman PR. Macromolecules 1983;16:589.
[4] Bakke JM, Bethell D. Acta Chem Scand 1992;46:644.
[5] Petermann J, Xu Y, Loos J, Yang D. Polymer 1992;33:1096.
[6] Yan S, Petermann J, Yang D. Colloid Polym Sci 1995;273:842.
[7] Yan S, Petermann J, Yang D. Acta Polym 1996;47:285.
[8] Yan S, Petermann J, Yang D. Polym Bull 1997;38:87.
[9] Lotz B, Wittmann JC. Makromol Chemie 1984;85:2043.
[10] Gross B, Petermann J. J Mat Sci 1984;19:105.
[11] Loos J, Katzenberg F, Petermann J. J Mater Sci 1997;32:1551.
[12] Lacroix Fv, Loos J, Schulte K. Polymer 1998;40:843.
[13] Martinez-Salazar J, Garcia Ramos JV, Petermann J. Int J Polym Mater 1993;21:111.
[14] Petermann J, Broza G, Rieck U, Kawaguchi A. J Mat Sci 1987;22:1477.
[15] Gall MJ, Hendra PJ, Peacock CJ, Cudby ME, Willis HA. Spectrochim Acta 1972;28A:1485.
[16] Strobl GR, Hagedorn W. J Polym Sci Polym Phys Ed 1978;16:1181.
[17] Naylor CC, Meier RJ, Kip BJ, Williams KPJ, Mason SM, Conroy N, Gerrard DL. Macromolecules 1995;28:2969.